EOMAP GmbH & Co.KG

Deutsches Zentrum für Luft- und Raumfahrt e.V.
in der Helmholtz-Gemeinschaft
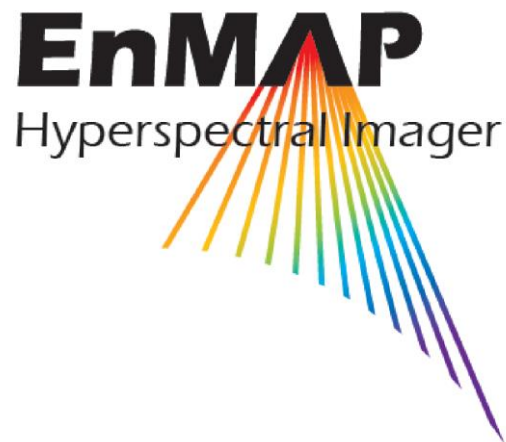
EnMAP Ground Segment

Level 2A Processor

(Atmospheric Correction Water) ATBD

Doc. ID	EN-PCV-TN-6008
Issue	3.1
Date	06.10.2022

Configuration Controlled: Yes

EnMAP
Hyperspectral Imager

German Remote Sensing Data Center (DFD)
Remote Sensing Technology Institute (IMF)
German Space Operation Center (GSOC)
EOMAP GmbH & Co.KG

-blank page -

TABLE OF SIGNATURES

Prepared

Date		Julian Wenzel
		EOMAP GmbH & Co.KG

Reviewed

Date		Thomas Heege
		EOMAP GmbH & Co.KG

Date		Rudolf Richter
		MF-PBA

Date		Raquel de los Reyes
		Subsystem Engineer Dev

Approved

Date		Emiliano Carmona
		System Manager PCV

Released

Date		Tobias Storch
		GS Project Manager

– blank page –

DISTRIBUTION LIST

This EnMAP Ground Segment document is stored in the Design Definition File (DDF) of the EnMAP Ground Segment Teamsite.

This document is accessible by all participants of the EnMAP Ground Segment as well as by the EnMAP Ground Segment Customer. This document may be further distributed by the EnMAP Project Management as necessary. After commissioning phase, the document is provided to the EnMAP user community on www.enmap.org.

TERMS AND DEFINITIONS

Terms, definitions and abbreviations for the EnMAP Ground Segment are collected together with those for the EnMAP Space Segment in a database which is publicly accessible via Internet on the EnMAP Information Portal:

http://www.enmap.org/

CHANGE RECORD

Version	Date	Chapter	Comment
0.9	30.09.2009	all	Draft Version
1.0	10.06.2010	all	First issue
1.1	02.11.2010	5	Answer to RID KAU-H-0211 included
1.2	29.04.2016	2.5	Ozone correction included due to a new requirement PCV-SR-3031-L2A-FUN
1.2	09.05.2016	2.5	Small corrections
1.3	1.12.2016	8	RIDs: FIS-S-0054. TBDs/TBCs are confirmed
1.3	1.12.2016	2.6.2.3	RIDs: FIS-S-0056
1.3	1.12.2016	2.5.2	RIDs: FIS-S-0063
1.3	1.12.2016	all	RIDs: GUA-L-0389
1.3	1.12.2016	2.4	RIDs: GUA-L-0390
1.3	1.12.2016	2.2	RIDs: HOL-A-0393
1.3	1.12.2016	2.7	RIDs: HOL-A-0394
1.3	1.12.2016	2.3	RIDs: HOL-A-0399
1.3	1.12.2016	2.4	RIDs: HOL-A-0401
1.3	1.12.2016	2.7	RIDs: HOL-A-0406
1.3	1.12.2016	2.6.2.3	RIDs: HOL-A-0408
1.3	1.12.2016	2.7	RIDs: HOL-A-0425
1.3	1.12.2016	2.5.1	RIDs: HOL-A-0426
1.4	23.03.2017	2.4	RIDs: GUA-L-0390
1.4	23.03.2017	5.1	RIDs: GUA-L-0390
1.4	17.07.2017	3.3	Chapter "Updating sensor data bases" is added
1.4	17.07.2017	5	Chapter is divided into two chapters 5.1 and 5.2
2.0	9.09.2019	2.3, 2.4, 2.5.1, 2.6.2.2, 2.7.1, 2.8	Algorithm update
2.0	26.11.2020	2.8	Updated quality control chapter
3.0	20.01.2022	all	Revised and completed Document for ORR
	06.10.2022	2.2	Changes in the cirrus harmonization with land processor during commissioning phase
	06.10.2022	all	Editorial changes
3.1	06.10.2022		Version for the FQR + CAR

Custodian of this document is Maximilian Langheinrich.

DOCUMENT PREPARATION

The EnMAP Ground Segment "Level 2A Processor Water" ATBD was prepared with contributions from EOMAP and DLR personnel as listed below.

First Name, Last Name	Organizational Unit / Chapters
EOMAP GmbH & Co.KG	
Julian Wenzel	2.4, 2.5.1, 2.6.2.2, 2.7.1, 2.8
Viacheslav Kiselev	all
Thomas Heege	Chapters 2.3, 2.8, 6, 7, references
German Remote Sensing Data Center / Deutsches Fernerkundungsdatenzentrum DLR-DFD	
Martin Bachmann	DFD-LA Chapters 2.8, 8
Rudolf Richter	DFD-LA Chapters 2.8, 8

EXTERNAL DOCUMENT REVIEW

Dr. Barbara Bulgarelli
Joint Research Centre (JRC) of the European Commission
TP 670, Via Fermi 1
21020 Ispra (VA), Italy

Reviewed on 9.06.2010
Comments from external review processed and included

– blank page –

CONTENTS

LIST OF FIGURES

LIST OF TABLES

1. Introduction

This ATBD describes the atmospheric correction algorithm of EnMAP data acquired over water surfaces. The algorithm converts the top-of-atmosphere radiances (level L1B or L1C) into underwater reflectances in the visible spectral interval. Underwater reflectances simply are the ratios of upward to downward fluxes right beneath the water surface. Normalized water reflectance is Upwelling Radiance divided by downwelling irradiance times pi for both nadir sun and nadir view angles. The L1B data can be processed before orthorectification and in this case VNIR and SWIR data must be co-registered to the VNIR spectrometer. Orthorectified data (L1C) can also be processed and in this case the nearest neighbor method should be applied for image resampling. Results of L2A Land processor (e.g. cloud mask and preliminary water mask) are also used as input to the L2A (water) processor.

The ATBD includes 9 sections. The first section (this section) specifies the aim of the document and its general structure. In the second section the detailed physical and mathematical description of the algorithms applied at different stages in the process of atmospheric correction of the images of water scenes is given. Section 4 contains the general processing scheme, showing the interfaces between the programming modules based on the algorithms of section 2. Section 5 describes how verification and validation of the presented algorithms is performed, section 6 defines the input and output data. The remaining sections contain technical information, facilitating the understanding of the document.

2. Algorithm description

2.1 Sun glitter mask formation

Sun glitter is the Fresnel's reflection from the water surface, which exists for a flat water surface only in a very short interval of observation angles. For a rough water surface, i.e. in the presence of waves, the interval of observation angles at which sun glitter contributes significantly to the upward radiance is much wider, so sun glitter can cover significant part of the scene and for the high-resolution data sometimes the whole scene. In the presence of sun glitter the part of the top-of-atmosphere radiance containing the information on the water bulk properties is very small resulting in high errors of the retrieval of water reflection. For that reason in the atmospheric processor for water scenes it is reasonable to mask out the areas with high sun glitter risk and to exclude them from processing. The developed algorithm aimed to specify the location of sun glitter affected areas follows.

Sun glitter detection is based on the Cox and Munk (1954) expression for the reflection coefficient of the rough water surface:

$$\bar{r}_c(\theta', \phi'; \theta, \phi) = \frac{1}{4\pi\sigma^2\mu^4} \frac{1}{cos\theta} R\left(cos\frac{\omega_r}{2}\right) exp\left(-\frac{1-\mu^2}{\mu^2\sigma^2}\right) \qquad (2.1.1)$$

where

$$\mu = \frac{cos\theta - cos\{\theta'}{2cos\frac{\omega_r}{2}} \qquad (2.1.2)$$

$$cos\omega_r = -cos\theta cos\theta' - sin\theta sin\theta' cos(\phi - \phi') \qquad (2.1.3)$$

Here R is the Fresnel's reflection coefficient of smooth water surface, θ' is the polar angle of the incident light, θ is the polar angle of the reflected light, ϕ' and ϕ are the azimuths of the incident and reflected light correspondingly. The incident beam is directed downward, the reflected beam is directed upward, so $cos\theta$ is always positive and $cos\{\theta'$ is always negative. The parameter characterizing the roughness of waved water surface in this formula is the dispersion of wave slopes σ^2. This value strongly depends on local conditions and no universal model for its calculation exists. For the open ocean σ^2 is usually assumed to depend linearly on wind velocity :

$$\sigma^2 = a + bw \qquad (2.1.4)$$

Different researches give different values of coefficients in this formula. According to Cox and Munk (1954):

$$a = 0.003 \quad b = 0.00512 \tag{2.1.5}$$

In MODIS algorithm (Gordon and Voss, 2004) the following values are used:

$$a = 0$$
$$b = 0.00273 \ (0.00246) \tag{2.1.6}$$

Two values for b are given as different dispersions in the direction of wind and in the transverse direction are adopted in this algorithm. The dispersions resulting from these two sets of coefficients are approximately the same for wind velocities at about 1.2 m/s. Cox and Munk (1954) values will be adopted in the EnMAP processor as the initial guess and refined at the commission stage.

As the analysis of satellite images shows, the expression (2.1.4) even for the open ocean can give only some average values of wind slope dispersion because of spatial and temporal variations of wind velocity and other wave generation conditions. In reality dispersion of wind slopes is highly variable and as a consequence the intensity of sun glitter is also variable. Correspondingly the formula (2.1.1) for the reflection coefficient of waved water surface can characterize only some average sun glitter intensity, not its exact value. For that reason the sun glitter phenomena in EnMAP processor will be characterized not by the intensity of sun glitter but by the probability of its appearance.

Let us rewrite the formula (2.1.1) in the form:

$$\frac{4\pi\mu^2(1-\mu^2)cos\theta \ \bar{r}_c(\theta',\phi';\theta,\phi)}{R\left(cos\frac{\omega r}{2}\right)} = \frac{1-\mu^2}{\mu^2\sigma^2} exp\left(-\frac{1-\mu^2}{\mu^2\sigma^2}\right) = \frac{d}{\sigma^2} exp\left(-\frac{d}{\sigma^2}\right) \tag{2.1.7}$$

For practical applications it is possible to approximate the function on the righthand side by the piecewise linear function:

$$z = xexp(-x) = \{0.3678x \quad 0 < x < 1 \quad 0.4578 - 0.09x \quad 1 < x < 5.087 \quad 0 \quad x > 5.087 \} \tag{2.1.8}$$

Substituting x by $\frac{d}{\sigma^2}$:

$$z = \left\{0.3678\frac{d}{\sigma^2} \quad \sigma^2 > d \quad 0.4578 - 0.09\frac{d}{\sigma^2} \quad \frac{d}{5.087} < \sigma^2 < d \quad 0 \quad \sigma^2 < \frac{d}{5.087}\right\} \tag{2.1.9}$$

The distribution of wind speed is well fitted by Weibull function (Sushama, 2007):

$$\Phi(w > w') = exp\left[-\left(\frac{w'}{c}\right)^k\right] \tag{2.1.10}$$

where $\Phi(w > w')$ is the probability of wind speed to be higher than a given value w' and the parameter k ranges between 1.8 and 2.3. For the present purpose the average value 2 can be adopted. In this case the function $\Phi(w > w')$ is called Rayleigh function:

$$\Phi(w > w') = exp\left[-\left(\frac{w'}{c}\right)^2\right] \tag{2.1.11}$$

Using the relationship (2.1.4) between w and σ^2 gives:

$$\Phi[\sigma^2 > (\sigma^2)'] = \left\{exp\left\{-\left[\frac{(\sigma^2)'-a}{bc}\right]^2\right\} \quad (\sigma^2)' > a \quad 1 \quad (\sigma^2)' < a\right\} \tag{2.1.12}$$

As follows from eq. (2.1.8), the value z as a function of σ^2 reaches maximum at $\sigma^2 = d$. Maximal value of z is 0.3678, so the probability for z to be higher than this value is zero. For lower values of z the probability for z to be higher than some value is the probability for σ^2 to be in the interval around the point of maximum:

$$\Phi(z > z') = \Phi[\sigma^2 > \sigma_1^2(z')] - \Phi[\sigma^2 > \sigma_2^2(z')] \tag{2.1.13}$$

where $\sigma_1^2 < d$ and $\sigma_2^2 > d$. The expressions for σ_1^2 and σ_2^2 are:

EnMAP Ground Segment

Level 2A Processor (Atmospheric Correction Water) ATBD

Restriction: Public

Doc. ID	EN-PCV-TN-6008
Issue	3.1
Date	06 Oct 2022
Page	13 of 39

$$\sigma_2^2(z') = \frac{0.3678d}{z'} \quad \sigma_1^2(z') = \frac{0.09d}{0.4578-z'} \tag{2.1.14}$$

These expressions are valid for $z' > 0$. For $z' = 0$ the probability $\Phi(z > 0) = 1$.

Parameter c of Rayleigh distribution is the average wind velocity. The detailed analysis of observations of surface winds from 723 weather stations over North America (Sushama, 2007) showed that for most types of underlying surface it is 3-4 m/s, increasing to 6-7 m/s only over the open water.

Due to the linear relationship between z and $\bar{r}_c$ the probability of sun glitter P_{glint}, i.e. the probability of surface reflection coefficient to exceed some value R_{glint}, is the probability of z to exceed the value:

$$z' = \frac{4\pi\mu^2(1-\mu^2)cos\theta \; R_{glint}(\theta',\phi';\theta,\phi)}{R\left(cos\frac{\omega_r}{2}\right)} \tag{2.1.15}$$

Eq. (2.1.13) gives the latter probability and correspondingly the probability of sun glitter P_{glint}.

The algorithm for the estimation of sun glitter probability includes the following steps:

a) estimation of z from (2.1.7) at the threshold value of water surface reflection $\bar{r}_c = R_{glint}$ for pixel sun and view angles;

b) estimation of threshold values of wave slope dispersions from (2.1.15)

c) estimation of sun glitter probability from (2.1.13)

Sun glitter increases the top-of-atmosphere radiance in all spectral intervals, but the most pronounced effect is observed in the infrared channels that distorts the results of the retrieval of atmospheric optical thickness and as a consequence the retrieved underwater reflectance. For that reason, the reflection of the waved surface must be compared with the reflection by the atmosphere in the infrared at 860nm. The apparent atmospheric reflectance in this spectral region does not exceed 5-6% for typical atmospheric conditions, so it is assumed to estimate the probability of water surface reflection to exceed R_{glint} =2%. Sun glitter is assumed to significantly influence the observations when the probability to exceed this value is higher than P_{glint} =30%.

2.2   Cirrus detection and correction

For the cirrus detection the measurements in both the near infrared region and the thermal infrared region of the solar spectrum can be used. As thermal infrared channels are absent in EnMAP, the use of near infrared channels is the only possibility. In bands with high water vapor absorption like this near infrared region the radiation reflected by the underlying surface is absorbed in the lower atmospheric layers, whereas the radiation reflected by cirrus clouds, located at high altitudes, is affected only by much lower absorption in the high layers, so cirrus pixels can be recognized based on higher signal level.

The strong water vapor band near 1.38 µm is successfully used for cirrus recognition in the MODIS processing chain (Gao et al, 2002). The simple threshold principle is applied: let us define the apparent reflectance as:

$$\rho = L\frac{\pi}{F_0 cos(\theta_0)} \tag{2.2.1}$$

where L is the sensor radiance, θ_0 is sun zenith angle and F_0 is solar irradiance. If for a given pixel ρ is larger than a given threshold, then cirrus is assumed to cover this pixel. The method requires that sufficient water vapor (> 1 cm) is present in the atmosphere; in this case cirrus pixels are recognized even over the land. This condition is mostly true: low humidity conditions can occur in polar regions, for high altitudes of underlying surface and in winter. All these situations are not typical for water scenes and for water surfaces this criterion is not so strict because of low surface reflectivity in the infrared.

The cirrus detection procedure in EnMAP at the first stage will be similar to that used for MODIS (Gao et al, 2002). The measured EnMAP channel radiances will be transformed into reflectance according to eq. (2.2.1); afterwards reflectance will be spectrally averaged to reduce the random errors:

$$\bar{\rho} = \frac{1}{N_2 - N_1 + 1}\sum_{i=N_1}^{N_2} \rho_i \tag{2.2.2}$$

where N_1 and N_2 are the first and the last channels over for the averaging is performed. The channels are selected in such a way that the center wavelength is about 1.375 μm and the wavelength difference between the first and last channels is about 30 nm. The cirrus masking from the land processor is used to identify cirrus pixels. If the number of cirrus pixels is bigger than 100, the cirrus correction is applied to all water channels of the scene. This is done in order to avoid stepwise changes along the edges of cirrus-clouds. Note that if the signal from the cirrus band is low, this yields low corrections. If the number of cirrus pixels is low, correction is skipped. Cirrus correction is based on the assumption that cirrus reflectance in each band $\rho_c(\lambda)$ is linearly connected to cirrus reflection at 1.38 μm(Gao et al, 2002):

$$\rho_c(\lambda) = \rho_c(1.38\mu m)/\gamma \tag{2.2.3}$$

where γ is determined from statistical processing of the scene. Neglecting cirrus absorption and scattering, the corrected reflectance is:

$$\rho_{cor}(\lambda) = \rho(\lambda) - \rho_c(1.38\mu m)/\gamma \tag{2.2.4}$$

.

The determination of the coefficient γ is based on the assumption that the reflectancies at the wavelength 1.38 μm and some other non-absorption channel depend on one another linearly if the reflection from the underlying surface does not contribute significantly to the top-of-atmosphere radiance. The coefficient at the linear term of this relationship is exactly γ. It is assumed that each scene contains enough pixels with low albedo of the underlying surface so that the following method of the determination of γ can be applied:

- pixels with a certain value of reflectance at 1.38 μm are selected and the minimal value of the reflectance at the reference non-absorbing channel is stored;

- this procedure is repeated for the set reflectance at 1.38 μm;

- the regression of reflectance at 1.38 μm on the minimal reflectances at the reference channels is built, the coefficient at the linear term gives γ.

A value of γ is calculated for all channels and used for correction. The parameter γ mainly depends on the solar and view geometry, and both change only by a very small amount for adjacent scenes, so stepwise changes at the borders of the scene resulting from the cirrus correction procedure are practically excluded.
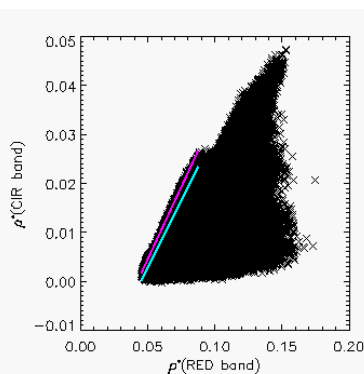

Figure 2-1: TOA reflectance scatterplot of the 1.38 μm cirrus band to red band

2.3 Adjacency correction

The adjacency effect results from horizontal diffusion of photons over an inhomogeneous underlying surface. If the underlying surface is partly covered by water the resulting radiance at the top of atmosphere when the sensor is oriented to the water can be written as:

$$L = L_{atm} + L_{wat}^{dir} + L_{wat}^{scat} + L_{land}^{scat} - L_{wl}^{scat} \qquad (2.3.1)$$

where L_{atm} is the radiance reflected from the atmosphere, L_{wat}^{dir} is the radiance reflected by water and reaching the sensor without scattering in the atmosphere, L_{wat}^{scat} is the radiance reflected by a horizontally homogeneous water surface and reaching the sensor after scattering in the atmosphere, L_{land}^{scat} is the radiance reflected by land and reaching the sensor after scattering in the atmosphere, L_{wl}^{scat} is the radiance reflected by water, covering the part of the surface where in reality is land, and reaching the sensor after scattering in the atmosphere. As the reflection coefficient of water surface is mostly lower than that of land (except maybe for some types of land cover in the blue region of the spectra, but in this case the adjacency effect is low in general), the last additive is small and can be neglected in practical calculations, so (2.3.1) can be written in the form:

$$\tilde{L} = L - L_{land}^{scat} = L_{atm} + L_{wat}^{dir} + L_{wat}^{scat} \qquad (2.3.2)$$

and as can be readily seen $\tilde{L}$ in this formula is the radiance which would reach the sensor observing the horizontally homogeneous water surface with the same properties as the original water basin surrounded by land. So after subtracting L_{land}^{scat} from the measured total radiance the algorithms for homogeneous water surface can be applied for the retrieval of underwater reflectance.

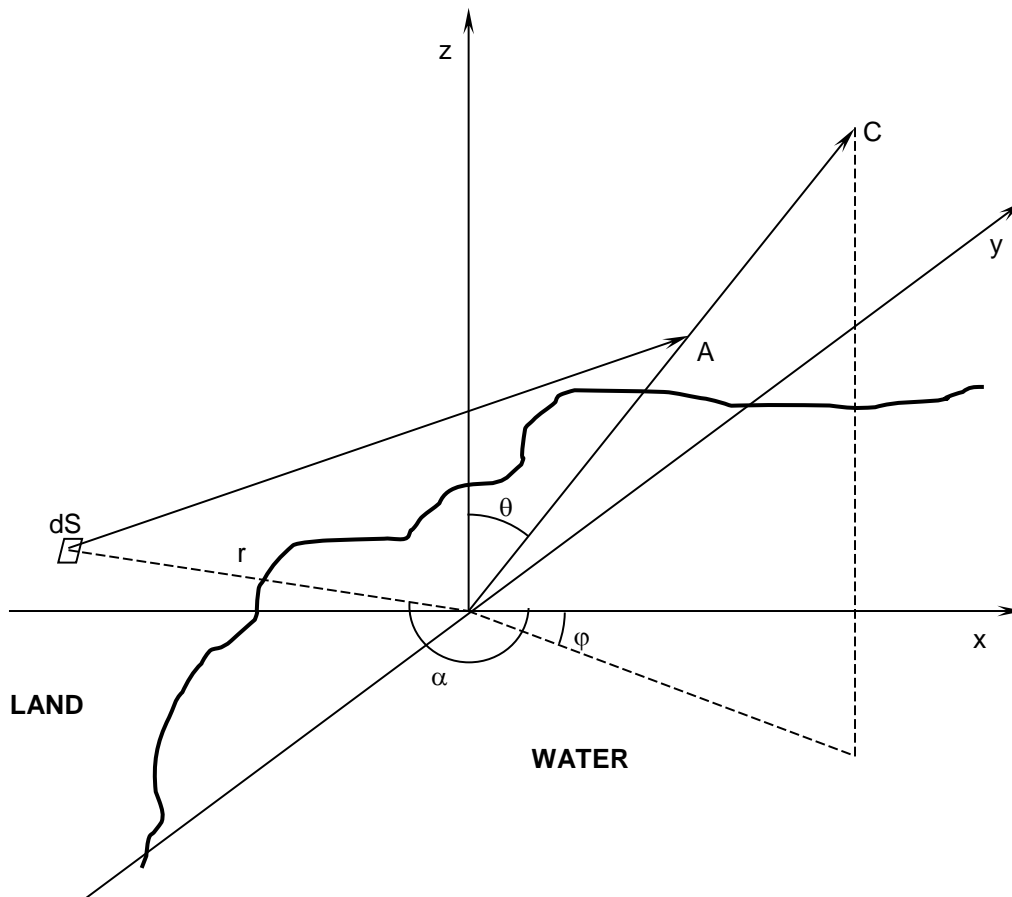Figure 2-2: The scheme of adjacency effect. The sensor is located in the point C, the scattering of the radiance reflected by the land surface element dS by the atmosphere occurs in the point A.

Let dS is the land surface element with coordinates (r, α), where r is the distance between dS and the point to which the sensor is oriented and α is the azimuth of the direction to the surface element. Let

$L'(r, \alpha; \theta, \phi)$ is the radiance reflected by dS and entering the sensor after reflection in the atmosphere from the direction defined by the view angle θ and azimuth ϕ (see fig. 2.2). With this notations L_{land}^{scat} can be written as:

$$L_{land}^{scat}(\theta, \phi) = \int_{\Omega_l} r dr d\alpha L'(r, \alpha; \theta, \phi) \qquad (2.3.3)$$

where the integration is performed over the area Ω_l covered by land. Normalizing (2.3.3) to the radiance $\bar{L}_{scat}^{land}(\theta, \phi)$, generated by reflection of homogeneous land surface with the same average reflectivity as the original surface and scattered in the atmosphere in the direction (θ, ϕ) gives:

$$L_{land}^{scat}(\theta, \phi) = \bar{L}_{land}^{scat}(\theta, \phi) \int_{\Omega_l} r dr d\alpha \, L'(r, \alpha; \theta, \phi)$$

$$L'(r, \alpha; \theta, \phi) = \frac{L'(r, \alpha; \theta, \phi)}{\int_{\Omega} r dr d\alpha L'(r, \alpha; \theta, \phi)} \qquad (2.3.4)$$

The integration in the denominator of the second formula is performed over the whole (x, y) plane. As the integration in (2.3.3 / 2.3.4) is performed over large areas and for that reason the small scale variations of land reflectance are damped, it is possible to substitute real radiances $L'(r, \alpha; \theta, \phi)$ by those resulting from reflection from the homogeneous land surface with average albedo. In this case $L(r, \alpha; \theta, \phi)$ does not depend on α and ϕ separately, but only on their difference. Fixing atmospheric conditions it is possible to introduce the new function $\hat{L}(r, \theta, \alpha - \phi)$:

$$\hat{L}(r, \theta, \alpha - \phi) = \int_r^\infty r' dr' L(r', \theta, \alpha - \phi) \qquad (2.3.5)$$
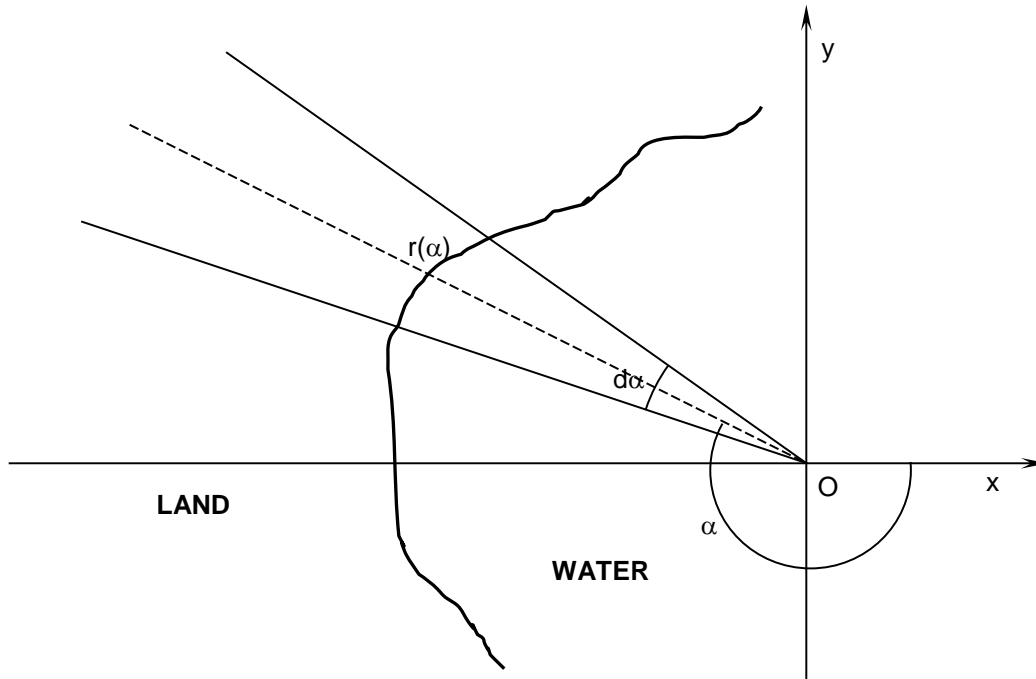
Figure 2-3: The scheme of adjacency effect parameterization. The sensor is oriented to the point O in the (x, y) plane.

In terms of this function the adjacency effect is written as (see fig. 2.3):

$$L_{land}^{scat}(\theta, \phi) = \bar{L}_{land}^{scat}(\theta, \phi\phi) \int_0^{2\pi} d\alpha \, \hat{L}(r(\alpha), \theta, \alpha - \phi) \qquad (2.3.6)$$

where $r(\alpha)$ is the distance from the observation point to the shore in the direction α. The expression becomes a bit more complicated in the case of intermittent land-water surfaces, e.g. for winding river or the bay of a complicated structure.

The estimation of $\hat{L}(r, \theta, \alpha - \phi)$ is based on the solution of the classical searchlight problem for the radiative transfer equation, i.e. the problem of scattering in the atmosphere of thin pencil of light. This problem is very difficult to exactly solve because of high dimensionality of the equation. However, it is possible to assume that the angular distribution of multiply scattered photons is close to the distribution

of photons experiencing only one collision with atmospheric constituents, so that the exact values of this function will be close to those obtained in the approximation of primary scattering. The searchlight problem in this approximation was earlier considered in (Rosenberg, 1962, Siewert, 1985, Santer & Schmechtig, 2000), but the expressions there are either not highly accurate or presented in the form that is difficult to use for further transformations. For that reason, the function $\hat{L}(r, \theta, \alpha - \phi)$ was obtained by directly solving the corresponding equation. For a horizontally homogeneous atmosphere the radiative transfer equation is:

$$(n, \nabla)I(\vec{r}, \vec{n}) = -\sigma(z)I(\vec{r}, \vec{n}) \frac{\kappa(z)}{4\pi} \int x(\vec{n} - \vec{n'}) \overrightarrow{I(\vec{r}, \vec{n'})dn'} \qquad (2.3.7)$$

Here $\vec{n}$ is a unit vector of the direction of radiation propagation, $\vec{r} = (x, y, z)$ is a vector of the observation point position, $\sigma(z)$ is the extinction coefficient, $\kappa(z)$ is the scattering coefficient, $x(\gamma)$ is the phase function,

$$\nabla = \vec{\imath} \frac{\partial}{\partial x} + \vec{\jmath} \frac{\partial}{\partial y} + \vec{k} \frac{\partial}{\partial z} \qquad (2.3.8)$$
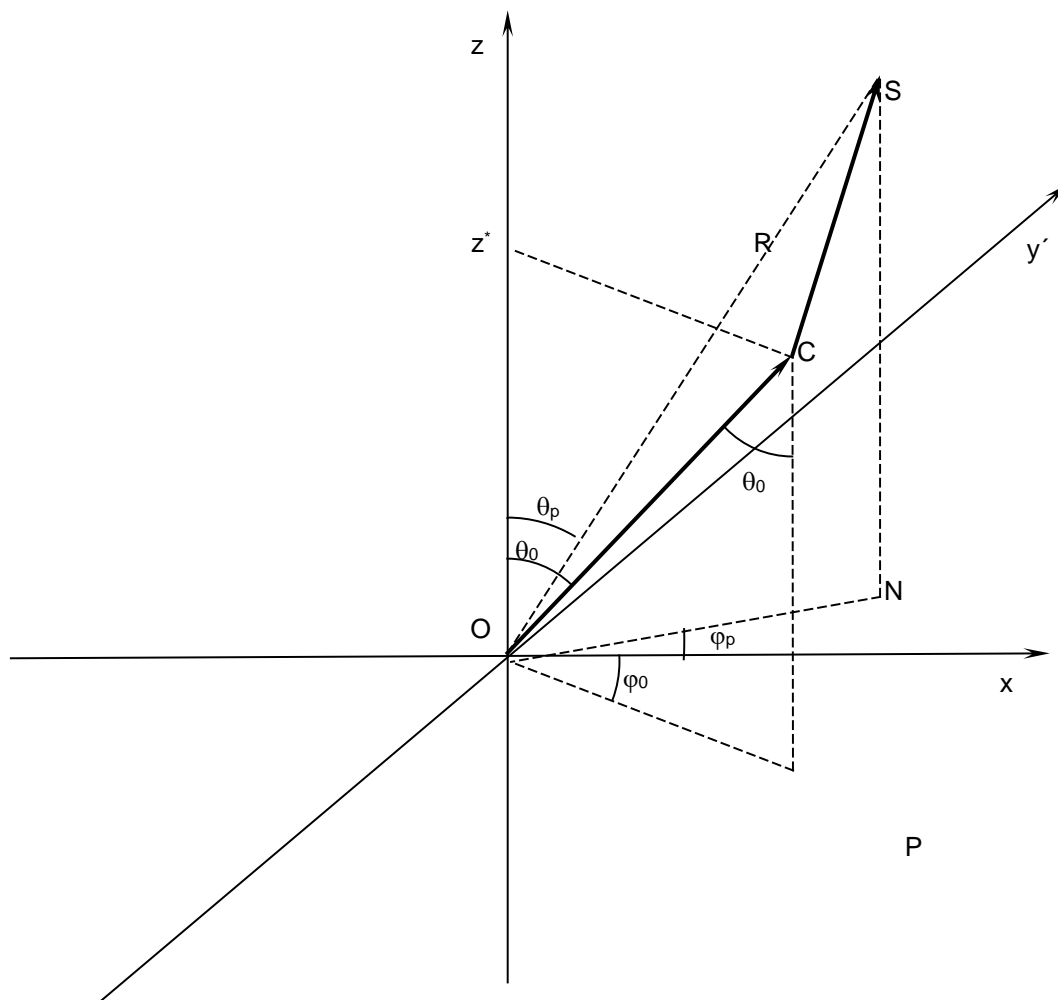

Figure 2-4: Coordinate system for the solution (2.3.11). The scattering occurs in the point C, the sensor is located in the point S, and the source is located in the point O.

The lower boundary condition for the searchlight problem is:

$$I(0, \vec{r}; \eta, \vec{n}) = \frac{S}{4\eta_0} \delta(\vec{r}) \delta[(\eta, \vec{n}) - (\eta_0, \vec{n}_0)] \qquad (2.3.9)$$

where $\eta_0, \vec{n}_0$ define the direction of the incident beam. Here it is assumed that Dirac's delta in the directional space is normalized as:

$$\frac{1}{4\pi}\int_{-1}^{1}d\eta \ \int d\vec{n} \ \delta[(\eta,\vec{n})-(\eta_0,\vec{n}_0)] = 1 \tag{2.3.10}$$

so the total radiation flux from the horizontal surface$(x,y,0)$ equals πS. The downward radiation at the top-of-atmosphere is assumed to be zero. The primary scattering approximation for the solution has the form:

$$I(R,\vec{n}_p,\vec{n},\vec{n}_0) = \frac{Sx(\vec{n}-\vec{n}_0)}{R}\eta_0\kappa(z^*)\exp\left[-\frac{1}{\eta_0}\int_0^{z^*}\sigma(z')dz'-\frac{1}{\eta}\int_{z^*}^{z}\sigma(z')dz'\right]\delta(\vec{n}\cdot[\vec{n}_p\vec{n}_0]) \tag{2.3.11}$$

for $0 < z^* < z$ and 0 in the other cases. Here z^* is:

$$z^* = R\eta_0\frac{\left([\vec{k}\times[\vec{n}\times\vec{n}_p]]\cdot[\vec{k}\times[\vec{n}\times\vec{n}_0]]\right)}{\left([\vec{k}\times[\vec{n}\times\vec{n}_0]]\cdot[\vec{k}\times[\vec{n}\times\vec{n}_0]]\right)} \tag{2.3.12}$$

$\vec{k}$ is a unit vector along $z$axis, $\eta_0 = \cos\theta_0$, $\vec{n}_p$ defines the direction to the sensor position, the sign "x" denotes vector product, the sign "." denotes scalar product, see other notations in fig. 2.4. The integrals in the exponent are the optical thicknesses of the layers from the surface to the scattering point and from the scattering point to the sensor:

$$\tau(z^*) = \int_0^{z^*}\sigma(z')dz'$$
$$\tau(z)-\tau(z^*) = \int_{z^*}^{z}\sigma(z')dz' \tag{2.3.13}$$

The formula (2.3.11) gives the intensity generated by the monodirectional source. As the land surface can be assumed to orthotropically reflect light, this expression must be integrated in θ_0 and ϕ_0 over the upper hemisphere:

$$I(R,\vec{n}_p,\vec{n}) = \int_0^{2\pi}d\phi_0\int_{\theta_p}^{\frac{\pi}{2}}d\theta_0\cos\theta_0 I(R,\vec{n}_p,\vec{n},\vec{n}_0) \tag{2.3.14}$$

Substituting L' in (2.3.4) by (2.3.14) gives L and further integration according to (2.3.5) gives the necessary function $\hat{L}$. This function is calculated according to the above formulae for the atmospheric parameters, defined as the result of preprocessing step (see section 3.1), and observation geometry for the tile. The dependence on r and ϕ is stored in the tabular form for the distances up to 50 km. The table is used for calculation of the contributions of reflections from the adjacent land to the apparent top-of-atmosphere reflectances from all water pixels in the tile.

The expression for the adjacency effect (2.3.6) includes also the radiance $\bar{L}_{scat}^{land}(\theta,\phi)$, generated by reflection of homogeneous land surface and scattered in the atmosphere in the direction (θ,ϕ). This radiance can be calculated from measured top-of-atmosphere radiances for land pixel. According to the assumption that real land surface can be substituted by homogeneous surface with average albedo, the radiances for land pixels surrounding considered water point are averaged (the size of the area for averaging will be discussed later), the resulting average radiance is denoted by $\bar{L}(\theta,\phi)$. The dependence of the top-of-atmosphere radiance $L(\tau,A;\theta,\phi)$ on aerosol optical thickness $\tau$and surface albedo A for each sensor channel is stored in the land database. For the fixed optical thickness (and aerosol type) the surface albedo can be retrieved. Then $\bar{L}_{scat}^{land}(\theta,\phi)$ can be calculated as:

$$\bar{L}_{land}^{scat}(\theta,\phi) = \bar{L}(\theta,\phi) - L(\tau,0;\theta,\phi) - \frac{AF^{\downarrow}(\tau,A)}{\pi}\exp\left(-\frac{\tau_{tot}}{\cos\theta}\right) \tag{2.3.15}$$

where $F^{\downarrow}(\tau,A)$ is the downward flux near the surface, and τ_{tot} is the total atmospheric optical thickness (including molecular component). The dependence of these values on parameters for each sensor channel is stored in the system in the flux database.

Summarizing the above, the algorithm of adjacency correction includes the following steps:
a) calculation of the average land top-of-atmosphere radiance;
b) retrieval of land reflected scattered radiance $\bar{L}_{land}^{scat}(\theta,\phi)$ according (2.3.15);
c) integration according (2.3.6) of contributions of land sectors, extracted from system tables;
d) subtraction of adjacency contribution from the water pixel top-of-atmosphere radiance.

The averaging in the item a) theoretically should be done for the whole land area, contributing to the apparent radiance of water pixel, i.e. contributing to the integral in the denominator of (2.3.4). However, as preliminary estimates show, the contribution of land areas located at distances up to several tenths

of kilometers is sometimes significant. To make the averaging over so large areas is not only time consuming but also technically impossible because of the restricted size of the scene. However, as the main contribution comes from the nearest land points and the land surface is statistically homogeneous, i.e. the average albedo varies slowly, it is reasonable to calculate the average over the restricted land area near the observation point and to extrapolate this value to larger distances. In land applications usually the circle of the radius about 1 km is used for the estimation of the average albedo. As the size of EnMAP pixel is about 1000 square meters, the averaging over 3-4 thousand pixels in the vicinity of observation point can be considered to lead to satisfactory results. The estimation of the contributions from the land surface outside the tile can be done if the land-water mask for the areas wider than the tile is supplied assuming the tile-average land albedo there. This approach is published in Kiselev et al. 2015 and tested operationally for thousands of high resolution satellite scenes (e.g. Landsat 5/7/8, Sentinel 2/3, MODIS, MERIS, Worldview 2/3 ..) and proved in most cases the reasonable results (e.g. Dornhöfer et al. 2018).

2.4 Retrieval of aerosol optical thickness

For each water pixel not covered by clouds (pixels marked by cirrus or haze flags are processed by the cirrus processor) two values are retrieved. Those values are τ and ASL and they are retrieved by minimizing the functional:

$$J = \sum_{i=1}^{N} \quad w_i \left\{ L_i^{(a)} - L_i^{(m)}(\tau, ASL) \right\}^2 \to min \qquad (2.4.1)$$

where $L_i^{(a)}$ are sensor radiances for the aggregated channel (see below), $L_i^{(m)}$ are modeled radiances for the same channels, w_i are channel weights, τ is the optical thickness at 550 nm and ASL is the aerosol slope (Miksa et al, 2004, Heege et al, 2009). Channel weights w_i here are selected according to the reliability of channels, i.e. low weights are set for the channels with high probability of error. Modeled radiances are assumed to be scene specific as the aerosol type is defined for each scene (see below). The aggregated channels radiances are the averages of sensor radiances in the neighbor original channels, i.e.

$$L_i^{(a)} = \frac{1}{N_i^{max} - N_i^{min} + 1} \sum_{j=N_i^{min}}^{N_i^{max}} L_j^{(s)} \qquad (2.4.2)$$

where $L_j^{(s)}$ are radiances in the original sensor channels. The aggregated channels are selected in the region of low atmospheric absorption and their width is varying in the limits 20 – 50 nm. The use of aggregated channels allows to reduce the random measurement error and to accelerate the retrieval whereas the accuracy of retrieval is not significantly influenced as the spectral dependence of aerosol optical thickness is a smooth function of wavelength. The set of aggregated channels include 11 channels in the VNIR region and 11 channels in the SWIR region. The spectral boundaries of aggregated channels are presented in the Table 2.1.

Table 2-1: Aggregated channels for the retrieval of aerosol optical thickness.

Low absorption spectral regions, nm	Aggregated channels, nm
400 - 670	400 – 430; 430 – 460; 460 – 490; 490 – 520; 520 – 550; 550 – 580; 580 – 610; 610 – 640; 640 – 670
835 - 895	840(835) – 860; 860 – 890
980 - 1080	990 – 1030; 1030 – 1080
1210 - 1300	1210 – 1260; 1260 – 1300
1520 – 1680	1530 – 1580; 1580 – 1630; 1630 – 1680

2070 – 2170	2070 – 2120; 2120 -2170
2210 - 2310	2210 – 2260; 2260 – 2310

The aerosol slope modifies the dependency of the total aerosol optical thickness on wavelength. In the database the standard maritime aerosol is stored. If the aerosol slope (ASL) is equal to 1, the standard wavelength dependency is used. For values different from one the τ for each channel is:

$$\tau = \tau_0 \, s_b \, (\lambda)^{-ASL} \tag{2.4.3}$$

where $s_b \, (\lambda)$ is the slope base for each wavelength.

When modeling aggregated channel radiances in the SWIR, infinite absorption is assumed. For VNIR channels absorption and backscattering are parametrized according to the formulae

$a_i = a_i^w + a \cdot a_i^s$ and $b_i = b_i^w + b \cdot b_i^s$. The coefficients a and b are obtained during the functional minimization. The specific absorption and scattering coefficients $a_i^w, a_i^s, b_i^w, b_i^s$ are constants and stored in the water optical property section.

2.5 Atmospheric correction

2.5.1 Retrieval of underwater reflectances

The underwater values of a and b are defined solving the equation

$$L_i^{(m)}(\tau, a_i^r, b_i^r) = L_i^s \tag{2.5.1}$$

Here $L_i^{(m)}$ is the modeled radiance for the channel *i,* and L_i^s is the sensor radiance for the channel *i* τ is the retrieved optical thickness for the pixel. The dependence of modeled radiance on corresponding parameters is extracted from the sensor water databases similar to Heege and Fischer, 2004.

From a and b, the underwater reflectance can be calculated by an analytical formula. This formula connects x = a / (b+a) to the subsurface irradiance reflectance R(x,Φ_{sun}), similar to Albert & Mobley 2003 but with modified coefficients:

$$R = (\alpha_1 + \beta_1 \cos(\phi_{sun})) \, x + (\alpha_2 + \beta_2 \cos(\phi_{sun})) \, x^2 + (\alpha_3 + \beta_3 \cos(\phi_{sun})) \, x^3 + (\alpha_4 + \beta_4 \cos(\phi_{sun})) \, x^4 \tag{2.5.2}$$

The coefficients are fitted using the FEM forward simulation for the full coupled water-atmospheric model (see chapter 2.7.1.), covering the widest ranges of water and atmospheric values over the whole available spectrum. x can be readily calculated from the total absorption and scattering values, the sun angle is an input parameter and R is simply the ratio of upward to downward flux right beneath the water surface. The data for the resulting combinations of sun angles, x and R were then fitted to the formula above.

Retrieval of normalized water leaving reflectance

The normalized water leaving reflectance is defined as ρ = Rrs(0, 0) * π. Rrs($\phi_{sun,}$ ϕ_{view}), the "remote sensing reflectance" is defined as the upwelling radiance Lu divided by the downwelling irradiance Ed. It depends on both (sun and view) angles. The normalized water leaving reflectance is the value of the

remote sensing reflectance times pi, that the exact water body under consideration would have if it was observed from a nadir angle with the sun in the zenith.

Similar to the underwater reflectance the FEM forward simulation for the full coupled water-atmospheric model is used to fit coefficients of the formula to connect this quantity to a and b.

$$\rho(x) = (\alpha 1)\, x + (\alpha 2)\, x2 + (\alpha 3+)\, x3 + (\alpha 4)\, x4 \qquad (2.5.3)$$

2.5.2 Correction of radiances for ozone absorption

The transfer of solar radiation in the interval 400-800 nm is influenced by the presence of molecular ozone in the atmosphere. This means that the dependence of modeled radiances on underwater reflectances in the equation 2.5.1 is different for different ozone concentrations. The effect of ozone absorption could be taken into account by introducing the value of ozone concentration as an additional parameter in the sensor databases. However, this approach would significantly increase the size of the databases. It is more efficient to use the fact that the bulk of the ozone concentration is located in the 20 – 30 km altitude region, while the main other atmospheric influence factors on the TOA radiance signal e.g. boundary layer and tropospheric aerosol, are located in the 0 – 10 km region. Therefore, as a good approximation, the ozone absorption can be de-coupled from the scattering (Richter et al. 2014). For example for a Lambertian surface reflectance ρ it is possible to write (Vermote et al. 1997, Richter and Schläpfer 2002):

$$L = T_{oz}\left(L_p + \frac{T\, E_g\, \rho/\pi}{1 - \rho\, s}\right) \qquad (2.5.4)$$

where L is the TOA radiance, T_{oz} is the ozone transmittance, L_p is the path radiance, T is the ground-to-sensor transmittance, E_g is the global (direct plus diffuse) solar flux on the ground, and s is the spherical albedo. The relative variation of the TOA radiance due to changes of ozone content relative to its standard value g_0

$$\Delta L(\theta, \theta', \lambda, g) = \frac{L(\theta,\theta',\lambda,g) - L(\theta,\theta',\lambda,g_0)}{L(\theta,\theta',\lambda,g_0)} \qquad (2.5.5)$$

does not depend on other atmospheric parameters and surface properties. This is because the dependence of the TOA radiance on the ozone concentration is present only in the form of a factor. Here θ and θ' are sun and view angles, λ is the wavelength, g is the ozone column content. These relative variations can be calculated by solving the radiative transfer equation and can be stored in look-up tables.

The correction of measured radiances $L(\theta, \theta', \lambda, g)$ for ozone absorption is performed by inverting the formula (2.5.4) for the calculation of the TOA radiance, which would occur if standard ozone column content existed:

$$L(\theta, \theta', \lambda, g_0) = \frac{L(\theta,\theta',\lambda,g)}{1 + \Delta L(\theta,\theta',\lambda,g)} \qquad (2.5.6)$$

The value $L(\theta, \theta', \lambda, g_0)$ is compatible with radiances stored in the sensor databases, so it can be used in the equation (2.5.1) for the retrieval of underwater reflectance.

As it is shown in (Richter et al. 2014), sufficient accuracy of the ozone correction is achieved if ΔL is stored in the form of linear regression on ozone column content:

$$\Delta L = a_0(\theta, \theta', \lambda) + a_1(\theta, \theta', \lambda)g \qquad (2.5.7)$$

and the coefficients a_0 and a_1 are stored over a 10 nm grid in wavelength in the interval 450-800 nm and a 10° grid in sun and view angles in the intervals 0-70° and 0-40° correspondingly with linear interpolation between the grid points.

The ozone content cannot be retrieved independently by ENMAP, so the ozone column information has to be taken from other sources, i.e. sensors dedicated to ozone measurements or corresponding ozone forecast models (Dobber et al. 2008, Loyola et al 2009). For ENMAP, which is a small field-of-view sensor, a single ozone value per tile (30x30 km) is appropriate, because the spatial ozone variation on a 100 km scale is low and global ozone measuring instruments have a coarse spatial resolution (typically 40 -100 km). This value can be also defined by the user. The standard ozone column content (330 DU) is used if no other information is available.

2.6 Water pixel detection

2.6.1 Theoretical basis for the detection of water pixels.

The main feature of water spectral signatures distinguishing it from clouds and land objects is low reflection in the infrared. In this region of the spectra the reflection coefficient even of the moist soils mostly exceeds 20% (see fig.2.5), being higher for clouds and other types of land surface, whereas the reflection coefficient of water bulk even for highly polluted basins is mostly lower than 0.1 (see fig 2.6). The appropriate spectral intervals for testing this property are 750-800 nm and 830-1800 nm.
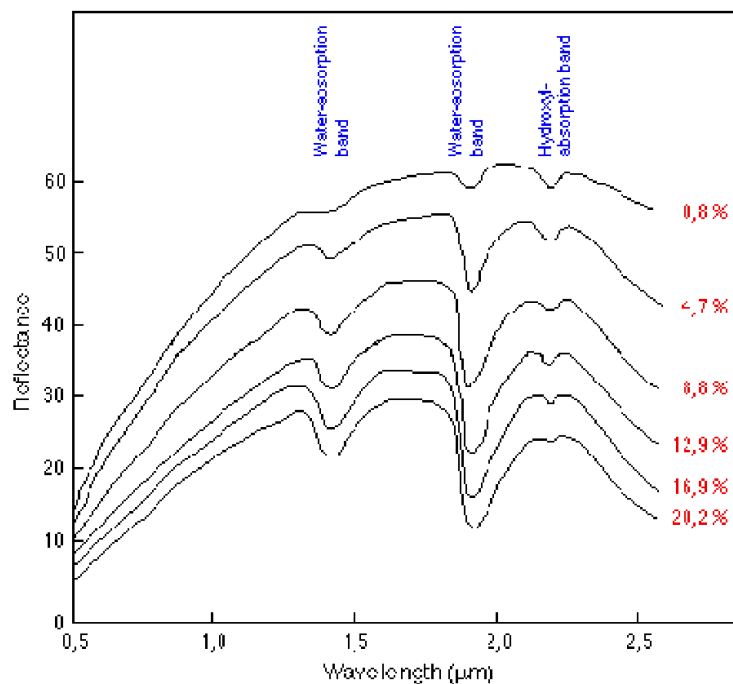
Figure 2-5: Soil reflection (silt loam) at different moisture content (after Bowers and Hanks, 1965).
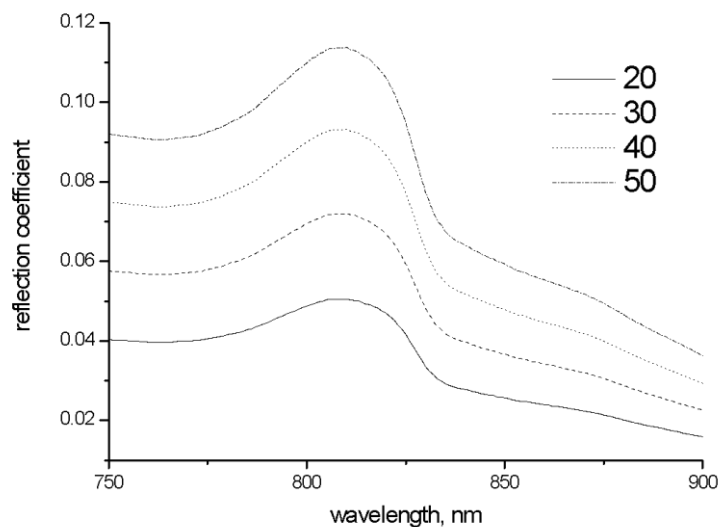
EnMAP Ground Segment
Level 2A Processor (Atmospheric Correction Water) ATBD
Restriction: Public

Doc. ID	EN-PCV-TN-6008
Issue	3.1
Date	06 Oct 2022
Page	24 of 39

Figure 2-6: Water bulk reflection coefficient for different concentrations of suspended matter[mg/l]. Sun zenith angle is 20□.

The other criterion for the detection of water pixels is the spectral trend of reflection coefficient in the region of "red edge", i.e. between 700 and 750 nm. Water reflection coefficient decreases here with wavelength whereas land reflection increases. The last feature is especially clearly expressed for the land covered with vegetation, but holds also for bare soil (fig. 2.7).
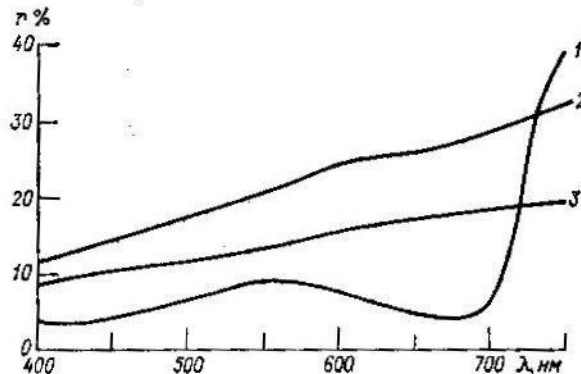
Figure 2-7: Reflection coefficients of mature vegetation (1), damaged vegetation (2) and soil (3) (after Kondratiev et al, 1986).

As absorption of light in the atmosphere attenuates the dependence of radiance at the top of atmosphere on surface reflectance, it is desirable to apply the first criteria in the spectral regions where atmospheric absorption is low or better negligible. The main absorbing component in the infrared region is water vapor (fig. 2.8). As it can be seen in the figure, the most appropriate spectral intervals are 740-800 nm, 820-900 nm, 1000-1080 nm, 1240-1280 nm and 1540-1640 nm. The use of lower wavelengths is preferable because of higher signal. The presence of oxygen absorption line at 760 nm restricts the application of the first of these intervals, but measurements at wavelengths higher than 770 nm can be used.
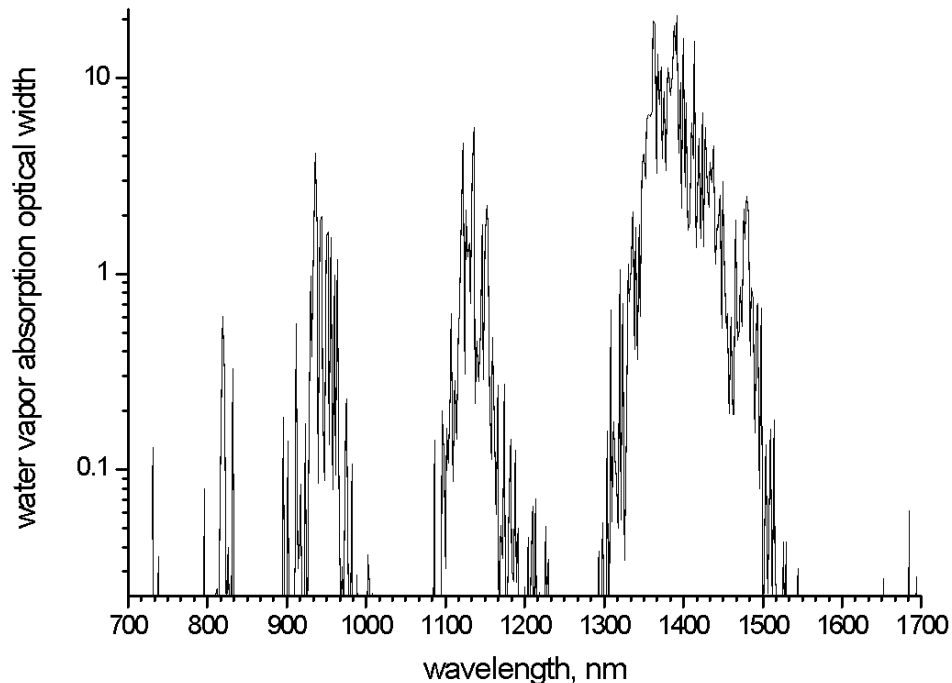
Figure 2-8: Water vapor absorption spectrum.

Application of the above criteria allows in most cases to reliably discriminate land and water pixels. The problem of misclassification, however, exists because of two effects: adjacency and shadows of clouds over the land. Horizontal diffusion of photons from surrounding land to the water surface leads to the rise of reflected radiation in the spectral region higher than 700 nm, resulting in the spectral trend similar to that of land surface, although significantly less expressed. As the spectral trend of the radiance reflected from the land in the cloud shadows has the same form as in the illuminated regions, but with significantly lower amplitude, the form of the spectra and the values of reflected radiance in the cloud shadows and over water in the shore region become very similar (see fig. 2.9). Although the radiance increase in the 700-750 nm region is slightly slower for water pixel, it does not give reliable basis for recognition. In these situations geometric criteria for the detection of cloud shadows must be used.

Figure 2-9: MERIS channel radiances for land pixel in the cloud shadow and water pixel near the shoreline.
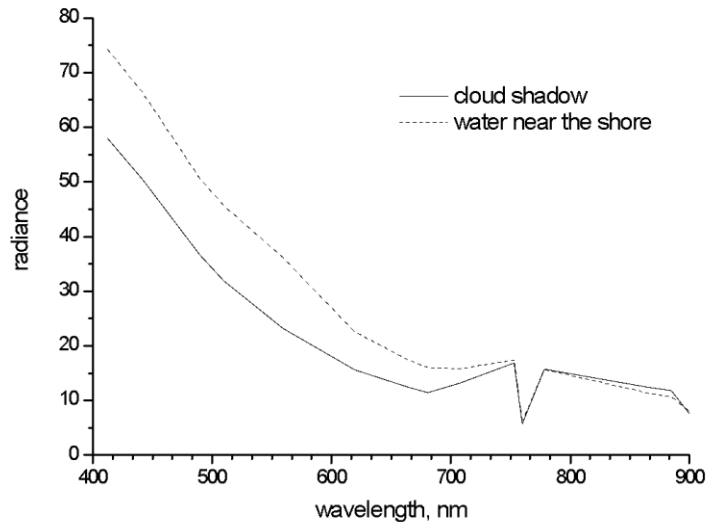

2.6.2 Algorithm of water pixel detection

2.6.2.1 Retrieval of surface reflection

Retrieval of surface reflection is performed using the EnMAP mission database, i.e. the database containing top of atmosphere EnMAP channel radiances for the selected set of atmospheric parameters and water bulk reflectance. Water bulk reflectance in this case is assumed to be orthotropic, molecular atmosphere is selected according to the season and latitude (MODTRAN classes), lower layer aerosol is maritime and its optical width is set to 0.1. Due to high values of land reflection the presence of Fresnel's reflection in the database can be neglected. The dependence of radiances for the channels used for water detection on water bulk reflectance for the above atmosphere is extracted from the database and the retrieval of surface reflection is just smooth interpolation of the inverse tabular dependence to the image pixel radiances.

As experiments with the existing satellite sensors showed, the sensitivity of the proposed criteria for water detection (see below) to the choice of aerosol type and optical width is low and this retrieval in most cases can be used for further steps. For reliability, on the basis of channel intensities at the highest wavelength used for water detection, the check of atmospheric aerosol optical depth value is made. The dependence of radiance for this channel on aerosol optical width for zero water bulk reflection is extracted from the EnMAP mission database and the aerosol optical width is interpolated to the radiance of the darkest 10% of detected water pixels. If the obtained value is larger than 0.35, the retrieval of surface reflectance is repeated with the obtained value of atmospheric optical width.

2.6.2.2 Water pixel recognition

The surface reflection values of four dedicated bands are used for the detection of water pixels. These bands are determined as closest valid band to the following wavelength: 480nm for the *Blue threshold*, 640nm for the *red threshold*, 860nm for the *IR threshold* and 1600nm for the *SWIR threshold*.

The detection follows a decision tree as shown in Figure 2-10:

The *Blue threshold* (0.3) checks for clouds; if the reflection in the blue is above this threshold the pixel is considered to be cloud or snow. However, if the infrared reflectance (*cloud IR threshold* in Figure 2-10) is low (<0.1), the pixel is still water. If the SWIR reflectance (SWIR snow *threshold* in Figure 2-10) is low(<0.05), the pixel is snow, if not, it is cloud.

The three thresholds *Red threshold* (0.25), *IR threshold* (0.15) and *water SWIR threshold* (0.08), check for land. If the pixel is above any of those thresholds, it can be considered as land. If all reflectances are lower than the respective thresholds, further checks can be performed.

The *IR cloud factor RED* and *IR cloud factor SWIR* (both 2.0) check for cloud shadows. If the infrared reflectance is brighter than both the IR and the SWIR reflectance by more than the respective factor, the pixel is considered a shadow pixel.

The *red slope threshold* (0.02) checks for mixed pixels, either coastal pixels or wet land surfaces fall in this category. If the IR Reflectance divided by the red reflectance below this threshold the pixel is water, or "strange land" the mixed pixel mentioned above.
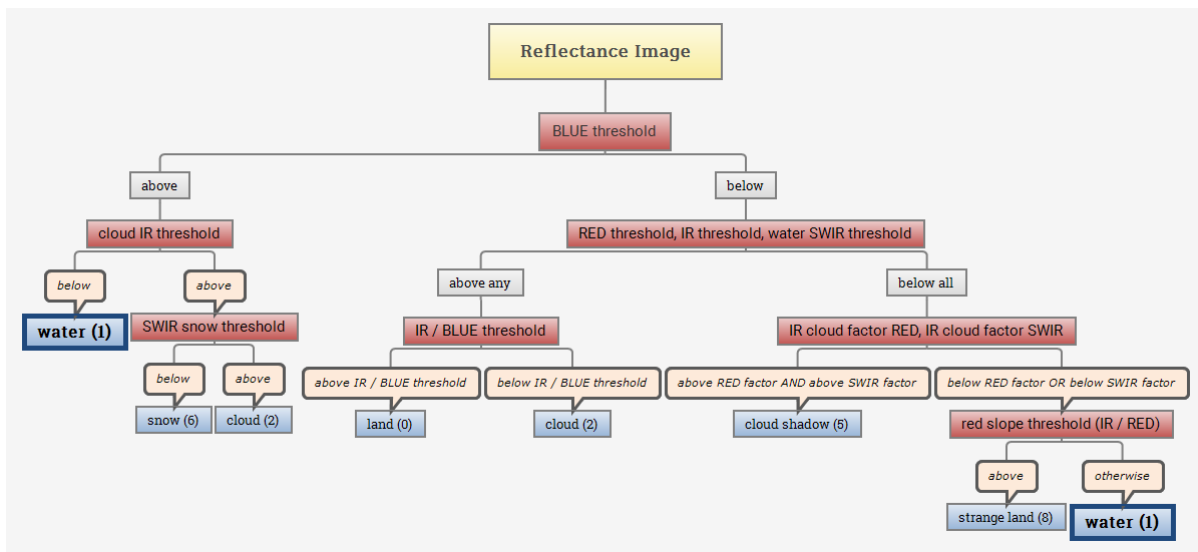

Figure 2-10: water pixel recognition workflow.

2.6.2.3 Check for misclassified pixels over land

As it is described in the previous section, pixels with low reflection can reliably be classified as water pixels or marked as dubious as low reflectance can be the result of pixel location in the cloud shadow. Cloud pixels are marked in the mask image, so the location of cloud shadow can be based on simple geometric arguments. The pixel is considered to be shadowed if the distance from the pixel to the closest cloud point in the direction to the sun is less than

$$L = Htan\theta_s \qquad (2.6.1)$$

where H is the cloud height and θ_s is the sun zenith angle. If it is found that a dubious pixel is in the cloud shadow, it is marked as land pixel and is not further treated by water processor. The reason for marking dubious a pixel as a land pixel is that its reflectances are higher than typical reflectances of a water pixel and the decrease of reflectances is caused by its low illumination. The cloud height is initially assumed to be 2 km and is further varied in the limits from 0.1 to 20 km. For each cloud height the sum

of radiances in the assumed shadow zone is calculated. The cloud height which gives the minimal sum of radiances is adopted for further calculations.

NOTE: Cloud shadows over water are neither detected nor corrected by this procedure. This check for cloud shadows will correct only the internal land-water mask for land pixels that were erroneously classified as water due to the impact of cloud shadow.

2.7 Radiative transfer databases

2.7.1 Monochromatic databases

MIP includes four monochromatic databases. These are L-database, containing upward radiances reflected by aquatic object, T-database, containing upward radiances reflected by land surface, F-database, containing downward fluxes and atmospheric optical characteristics. Radiances in these databases are normalized per unit solar flux. Spectral resolution is defined in the process of program initialization, 10 spectral intervals with different resolution can be defined in the spectral region from ultraviolet to microwave frequencies. For the EnMAP application the monochromatic databases are created with the resolution 0.5-1 nm. The following set of parameters defines radiance values in the L-database:

- solar zenith angle,
- view zenith angle,
- azimuth difference between view direction and direction to the sun,
- optical depths of four aerosol types (urban, maritime, rural and tropospheric),
- surface altitude,
- scattering of the water body
- absorption of the water body

The last parameter simulates the reflectivity of water bulk.

Parameters of T- and F- databases are:

- solar zenith angle,
- view zenith angle,
- azimuth difference between view direction and direction to the sun,
- optical depths of four aerosol types (urban, maritime, rural and tropospheric),
- surface altitude,
- surface albedo.

The set of points in the parameter grid of these databases can be arbitrarily varied both at program initialization and in the process of program functioning. The temperature and salinity impact is below 1% and therefore negligible for the bidirectional considerations.

All databases are created by solving the radiative transfer equation for the plane-parallel multilayer atmosphere using the finite element program (Kiselev et al, 1994, Bulgarelli et al, 1999):

$$\eta \frac{\partial L(\tau,\eta,\phi;\lambda)}{\partial \tau} = -L(\tau,\eta,\phi;\lambda) + \frac{\Lambda(\lambda)}{4\pi}\int_{-1}^{1} d\eta' \int_{0}^{2\pi} d\phi' x(\gamma,\lambda)L(\tau,\eta',\phi';\lambda) + Q(\tau,\eta,\phi;\lambda) \qquad (2.7.1)$$

where τ is the optical depth, η is the cosine of polar angle and ϕ is the azimuth of radiation propagation, Λ is the single scattering albedo, $x(\gamma,\lambda)$ is the phase function, γ is the scattering angle, λ is the wavelength, Q is the source term, generated by first-order scattering of the solar beam.

Over water this equation is solved for light propagation in both atmosphere and water media, taking into account Fresnel's reflection at the air-water interface. Boundary conditions and the source term for deep water are:

$$L(\tau,\eta,\phi;\lambda)|_{\tau=0} = 0$$

$$L^\uparrow(\tau-0,\eta,\phi;\lambda)|_{\tau=\tau_a} = T^\uparrow(\eta_r,\lambda)L^\uparrow(\tau_a+0,\eta_r,\phi;\lambda) + R^\downarrow(\eta,\lambda)L^\downarrow(\tau_a-0,\eta,\phi;\lambda) \; L^\downarrow(\tau+0,\eta_r,\phi;\lambda)|_{\tau=\tau_a} =$$
$$T^\downarrow(\eta,\lambda)L^\downarrow(\tau_a-0,\eta,\phi;\lambda) + R^\uparrow(\eta_r,\lambda)L^\uparrow(\tau_a+0,\eta_r,\phi;\lambda) \qquad (2.7.2)$$

$$L(\tau,\eta,\phi;\lambda)|_{\tau\to\infty} \to 0$$

$$Q(\tau,\eta,\phi;\lambda) = \frac{\Lambda(\lambda)}{4}\left[x(\gamma_0^+,\lambda)exp\left(-\frac{\tau}{\eta_0}\right) + x(\gamma_0^-,\lambda)exp\left(-\frac{2\tau_a-\eta}{\eta_0}\right)\right] \quad for \; \tau < \tau_a \; Q(\tau,\eta,\phi;\lambda) =$$
$$\frac{\Lambda(\lambda)}{4}T^\downarrow(\eta_0,\lambda)x(\gamma_0^w,\lambda)exp\left(-\frac{\tau_a}{\eta_0}\right)exp\left(-\frac{\tau-\tau_a}{\eta_0^w}\right) \quad for \; \tau > \tau_a \qquad (2.7.3)$$

where

$$cos\gamma_0^+ = \eta\eta_0 + \sqrt{1-\eta^2}\sqrt{1-\eta_0^2}cos(\phi-\phi_0) \; cos\gamma_0^- = -\eta\eta_0 + \sqrt{1-\eta^2}\sqrt{1-\eta_0^2}cos(\phi-\phi_0) \; cos\gamma_0^w =$$
$$\eta\eta_0^w + \sqrt{1-\eta^2}\sqrt{1-(\eta_0^w)^2}cos(\phi-\phi_0) \qquad (2.7.4)$$

T and R are Fresnel's transmission and reflection coefficients of air-water interface, the upper indices "↓" and "↑" denote downward and upward directions of radiation propagation, τ_a is total optical thickness of the multilayer atmosphere, η_r is the cosine of refracted angle of radiation propagation, η_0 and η_0^w are polar angles of solar beam in the atmosphere and water correspondingly, ϕ_0 is the azimuth of solar beam. Transmission and reflection coefficients are calculated taking into account the spectral dependence of the water refractive index according to (Segelstein, 1981, Pope & Fry, 1997). For the shallow water case the lower boundary conditions are similar to those for the land surface.

Boundary conditions and the source term over land are:

$$L(\tau,\eta,\phi;\lambda)|_{\tau=0} = 0$$

$$L^\uparrow(\tau,\eta,\phi;\lambda)|_{\tau=\tau_a} = \frac{A}{\pi}\int_0^1 d\eta' \int_0^{2\pi} d\phi'\eta'L^\downarrow(0,\eta',\phi';\lambda) \qquad (2.7.5)$$

$$Q(\tau,\eta,\phi;\lambda) = \frac{\Lambda(\lambda)}{4}x(\gamma_0^+,\lambda)exp\left(-\frac{\tau}{\eta_0}\right) \qquad (2.7.6)$$

where A is the surface albedo.

Atmospheric optical properties are calculated for the given set of database parameters according to the MODTRAN model (Abreu & Anderson, 1996). Water optical properties are modelled using spectral dependencies of specific optical properties of water constituents, namely chlorophyll, suspended matter and yellow substance. These dependencies are tabulated and stored in the system in ASCII files.

Monochromatic databases are created at system initialization (although certain modifications are possible when program is already used in a routine regime). The need to rebuild these databases may arise only if improvement of atmospheric or water model becomes necessary.

2.7.2 Sensor databases

Sensor databases contain the same values as monochromatic databases but spectrally averaged over the channel sensitivity interval. For each monochromatic database a corresponding sensor database is created, parameterized in the same way as original monochromatic database. As distinct from monochromatic databases, sensor databases contain real radiances, which take into account spectral variations of solar constant, i.e. radiances in the sensor database are obtained from radiances in the monochromatic database according to the formula:

$$L_i^{sb} = \int d\lambda \; r_i(\lambda)S(\lambda)L^{mb}(\lambda) \qquad (2.7.7)$$

where i is the channel number, $r_i(\lambda)$ is the channel response function, $S(\lambda)$ is the solar constant, L^{mb} is the radiance of monochromatic database (other parameters are omitted for brevity). The integration is performed theoretically over all real values, but practically over the interval where the response function of the channel is different from zero. Other values are just averaged over the channel wavelength interval:

$$z_i^{sb} = \int d\lambda \; r_i(\lambda)z^{mb}(\lambda) \qquad (2.7.8)$$

where $z^{mb}(\lambda)$ is the value of the monochromatic database.
Sensor databases are rebuilt after rebuilding of monochromatic databases and if essential variation of channel response functions occurs.

2.8   Data quality control

In order to assess the quality of each pixel in the retrieval, each pixel is checked after the retrieval and an overall pixel quality Q is calculated for each water pixel. The values range from 0 for lowest quality to 1 for high quality indication. The total quality is the product of all sub-quality markers Q_i , where each of them has values again between 0 and 1.
We define quality markers for the sun elevation Q_s, the aerosol AOT value Q_a, the aerosol slope value Q_l and the sunglitter risk Q_{sgl} .The **total quality** is then defined by:

$$Q = Q_s * Q_a * Q_l * Q_{sgl}$$
(2.8.1)

For each of those values there is a value at which the quality reduction starts, and a value at which the quality is 0. In between the quality decreases linear. Accordingly, the sun elevation quality marker is linear reduced for high sun angles from 55° to 65° deg, the AOT value marker for high values of AOT from 0.3 to 0.7 AOT, and the slope marker for extreme slopes (<0 to -0.5 or >2 up to 2.5) as shown in Figure 2-11. The sunglitter quality marker is calculated using equation 2.1.1 (reference MIPL-TN-SCT-002 2017) with a lower thresholds at 2% according to EN-GS-TN-6003 (2018) and up to 8% for Q_{sgl} =0. The highest sunglitter reflectance value for wind speeds of 3 and 8m/s is used.
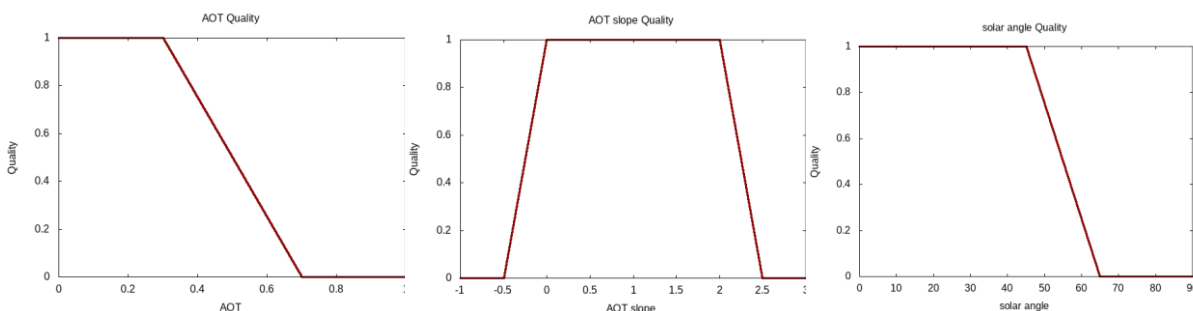
Figure   2-11: data quality for different functions for different parameters

As described in EN-PCV-DD-8004 and EN-PCV-TN-8005, data quality control is also conducted for atmospherically-corrected data (L2A).

The quality of atmospheric correction is likely to be reduced when further diminishing environmental conditions occur. Parameters for such conditions include:

- Percentage of water pixels influenced by sun glitter [> 10%: low quality]
- Percentage of haze (> 20%: low quality)
- Percentage of clouds (> 20%: low quality)

3. Program modules and interfaces. Processing scheme

Processing of water scenes in EnMAP consists of two steps: a) preprocessing step and b) main processing step. Preprocessing step is obligatory performed for all scenes of the satellite trajectory and after that the main processing step begins. Such organization of processing is required because of the necessity of smooth interpolation of aerosol type at the scene boundaries (see the section "Retrieval of aerosol optical thickness").

3.1 Preprocessing step.

The results of this step are sent for permanent storing to the system and used at the main processing step both for catalog order and acquisition request.

Input: radiance cubes and cloud masks of land processor for all scenes on the trajectory.

Output: aerosol type, aerosol optical thickness of the scene, percent of water pixels non-affected by sun glitter, corrected water mask and sun glitter map for each scene on the trajectory.

1. Sun glitter map generation.
Sun glitter map is generated in the core memory and is stored only if for at any rate one pixel of the scene the probability of sun glitter (wave reflection coefficient greater than R_{glint}) exceeds P_{glint}. See algorithm description for more details.

2. Correction of water mask
The new values of water mask are generated using the algorithm of the section "Water pixel detection" and compared with the water mask from the level 1. Pixels not affected by sun glitter are corrected, pixels affected by sun glitter (probability of sun glitter exceeds P_{glint}) are not modified. If the scene contains no water pixels or all water pixels are affected by sun glitter, the scene is marked as non-appropriate for processing in water mode, processing stops, no water masks are produced for this scene, aerosol type and optical thickness are set to "not defined" values. Percent of water pixels non-affected by sun glitter is calculated.

3. Formation of cirrus mask
Cirrus mask is formed according to the algorithm in this document.

4. Search of dark water pixels
Pixels marked as cloud, haze, cirrus, bad or influenced by sun glitter are excluded from the search. Pixel is added to the list of dark pixels if it is darker than the others at any rate in one of SWIR channels. The number of used water pixels in the scene is calculated.

5. Formation of aggregated channels
If the number of used water pixels is less than 1% of the total number of scene pixels, rural aerosol type and aerosol optical thickness 0.1 are set for the scene, the execution of the program stops. In the opposite case dark pixel channel radiances are averaged. Aggregated channels are formed for the averaged radiances according to the aggregated channel list in the section "Retrieval of atmospheric optical thickness" for the averaged dark pixel.

6. Selection of aerosol type
Aerosol type for the averaged dark pixel is defined for the scene according to the algorithm in the section "Retrieval of atmospheric optical thickness".

7. Retrieval of AOT for the scene
Aerosol optical thickness is retrieved for the averaged dark pixels according to the algorithm in the section "Retrieval of atmospheric optical thickness".

Figure 3-12: The scheme of processing step

3.2 Main processing step

This step is performed for each scene. After processing for the catalog order the quality characteristics are sent for permanent storing in the system, after processing for acquisition request all output data are sent to the user.

Input: radiance cube, water, cloud and sun glitter masks for the scene, aerosol types for all scenes on the trajectory.

Output: underwater reflectance cube, corrected cloud mask and quality data for the scene, map of atmospheric optical thickness over water.

1. Cirrus correction.

This operation is performed for all water pixels not covered with clouds and not affected by sun glitter according to the algorithm in the section "Cirrus detection and correction"

2. Adjacency correction.

This operation is performed for all water pixels not covered with clouds and not affected by sun glitter according to the algorithm in the section "Adjacency correction"

3. Formation of aggregated channels

This operation is performed for each pixel according to the aggregated channel list in the section "Retrieval of atmospheric optical thickness". Only water pixels not covered with clouds and not affected by sun glitter are processed.

4. Retrieval of aerosol optical thickness.

This operation is performed for each pixel according to the algorithm in the section "Retrieval of aerosol optical thickness". The next step begins after the retrieval of aerosol optical thickness for all appropriate pixels in the scene.

5. Correction of cloud mask.

Water pixels at cloud edges for which the retrieved aerosol optical thickness is higher than τ_{cloud} are marked as cloud pixels.

6. Atmospheric correction.
7. The step is performed for all water pixels not covered with clouds and not affected by sun glitter. Data quality control.

Quality characteristics of the scene according to the algorithm in the section "Data quality control" are calculated.

3.3   Updating sensor data bases

The precondition of any MIP program runs is the availability of the sensor database. Any change of the ENMAP spectral response function requires to rebuild the sensor data base from the main data base (see chapter 2.7.2). Furthermore, sensor databases are rebuilt after rebuilding of monochromatic databases.

Input: Sensor spectral response function, Monochromatic databases

Output: sensor databases, see 2.7.2

The monochromatic databases (chapter 2.7.1.) are created by EOMAP only once at system initialization and remain over the sensor lifetime. The need to rebuild these databases may arise only if improvement of atmospheric or water model becomes necessary.

4.   Algorithm verification and validation

The main part of algorithms (water mask, optical thickness retrieval, atmospheric correction) was tested and verified using the images of many existing sensors, i.e. MERIS, MODIS, SPOT, LANDSAT, ASTER, QUICKBIRD, CHRIS-PROBA, etc. Verification is permanently continuing and algorithms are improved for providing robust and reliable results.

The algorithm is being validated with the help of AERONET data at multiple stations. This is done for AOT and water reflectances. Results are still pending.

The spectral region from 0.9 to 1 um contains overlapping channels from the VNIR / SWIR spectrometers. All channels will be processed and delivered to the user, but an inter-spectrometer re-calibration will be necessary if TOA radiance offsets exist between overlapping channels. This investigation is part of the commissioning phase and the Principal Investigator and DLR Space Agency shall come to an agreement to recommend a corresponding requirement.

Atmospheric correction of water pixel top-of-atmosphere radiances is performed for each sensor channel.

5. Input/Output data

5.1 Generation of LUT's / sensor database

5.1.1 Input data

- Sensor spectral response function, Monochromatic databases

5.1.2 Output data

- Sensor database / LUT

5.2 Processor

5.2.1 Processor input data

For each scene:
- radiance cube, ENVI BIL format;
- observation geometry: sun polar angle and azimuth (clockwise from the North), sensor view angle and azimuth (clockwise from the North), scene geographic coordinates; all data for the center of the scene and scene corners;
- waterType - the parameter on water turbidity. The default value is "turbid" as per "Processor Design Document" EN-PCV-DD-2004, Issue 1.3, 12 Dec 2016.

Sensor definition
- sensor FOV,
- number of pixels per line,
- number of channels,
- channel response functions

Radiative transfer databases and adjacency contribution tables (see corresponding sections)

Global land/water mask

5.2.2 Processor output data

Permanently stored in the system
- sun glitter map for the scene
- corrected mask including quality flag per pixel for the scene (only water pixels)
- Total quality per pixel QUT (only water pixels), quantifying the overall quality of each pixel from low to high from 0-1
- Quality data (percent of water pixels, percent of clear water pixels, average aerosol optical thickness for water pixels)

Generated by request
- underwater reflectance/normalized water reflectance cube for the channels in the visible region of the spectra,
- pixel map of aerosol optical thickness (over water)
- log file of optical thickness retrieval and atmospheric correction.

6. Summary

The algorithms of water scene processing in this document are based on fundamental physical principles that provides for their reliability and robustness. The main part of algorithms (water detection, retrieval of optical thickness, atmospheric correction) were tested for various satellite sensors (MERIS, MODIS, LANDSAT, SPOT and others) and demonstrated their effectiveness. New items in the processing chain are the adjacency correction algorithm, pixelwise aerosol and aerosol-slope determination, and improved atmospheric transformation algorithm and improved quality control mechanisms for each pixel. The tuning of algorithms to the specific sensor characteristics consists in the modification of a small set of predefined constants and in application to the EnMAP sensor can be easily performed in the commissioning phase.

7. References

Abreu L. W. and Anderson G. P. "The MODTRAN 2/3 Report and LOWTRAN 7 Model", *Ontar Corporation*, 260 p. (1996)

Bowers, S.A., Hanks R.J. "Reflection of Radiant Energy From Soils", Soil Science. 100(2):130-138 (1965)

Bulgarelli B., Kisselev V. and Roberti L. "Radiative transfer in the atmosphere-ocean system: the finite element method", *Appl. Opt.*, 38, pp. 1530-1542 (1999)

Cox C, Munk W. "Some problems in optical oceanography", *J. Marine Res*,14, pp. 63-78 (1954)

Dörnhöfer, K., Klinger, P., Heege, T., Oppelt, N.: Multi-sensor satellite and in situ monitoring of phytoplankton development in a eutrophic-mesotrophic lake. Science of the Total Environment 612C (2018) pp. 1200-1214 DOI information: 10.1016/j.scitotenv.2017.08.219

Dobber, M., Kleipool Q., Dirksen R., Levelt P., Jaross G., Taylor S., Kelly T., Flynn L., Leppelmeier G., and Rozemeijer N. "Validation of Ozone Monitoring Instrument Level 1b Data Products." *Journal of Geophysical Research,* 113, D15S06 (2008) doi:10.1029/2007JD008665.

EN-GS-TN-6003 Sunglint Avoidance Strategy, DLR EnMAP Ground Segment 8.3.2018

EN-PCV-DD-8004 Quality Control Design Document

EN-PCV-TN-8005 HSI Geometric Calibration and Quality Control Concept

Heege, T., Fischer, J. "Mapping of water constituents in Lake Constance using multi-spectral airborne scanner data and a physically based processing scheme", *Can. J. Remote Sensing*, 30(1), pp. 77–86 (2004)

Heege, T., Viacheslav, K., Odermatt, D., Heblinski, J., Schmieder, K., Khac, T.V., Long, T.T.: "Retrieval of water constituents from multiple earth observation sensors in lakes, rivers and coastal zones, Proc. IEEE Int. Geoscience and Rem. Sens. Symp., Cape Town (2009)

Gao, B.-C., Yang, P., Han, W., Li, R.-R., and Wiscombe, W. J., "An algorithm using visible and 1.38 µm channels to retrieve cirrus cloud reflectances from aircraft and satellite data", *IEEE Trans. Geosci. Rem. Sens.*, 40, 1659-1668 (2002).

Gordon H.R. and Voss K.J.," MODIS Normalized Water-leaving Radiance", *ATBD-MOD*-18 (2004)

Kiselev, V., Roberti L. and Perona G. "An Application of the Finite Element Method to the Solution of the Radiative Transfer Equation", *J. Quant. Spectr. Radiat. Transfer*, 51, pp.603--614, (1994)

Kiselev, V., Bulgarelli, B. and Heege, T.. Sensor independent adjacency correction algorithm for coastal and inland water systems. Remote Sensing of Environment, 157: 85-95., ISSN 0034-4257, http://dx.doi.org/10.1016/j.rse.2014.07.025. (2015)

Kondratiev K.Ya., Kozoderov V.V., Fedchenko P.P. "Aerospace studies of soil and vegetation" (in Russian), *Gidrometeoizdat*, Leningrad, 231 p. (1986)

Loyola, D. G., Coldewey-Egbers R. M., Dameris M., Garny H., Stenke A., Van Roozendael M., Lerot C., Balis D., and Koukouli M. "Global Long-Term-Monitoring of the Ozone Layer – a Prerequisite for Predictions." *International Journal of Remote Sensing*, 30, pp. 4295–4318 (2009)

Miksa, S., Heege, T., Gege, P., Kisselev, V. "Coupled Aerosol and Water Constituent Retrieval Algorithm for Hyperspectral Remote Sensing Sensors over Case II Water Lake Constance", *SPIE Proc. Ocean Optics XVII, October 25-29, Fremantle*, *CD-ROM proceedings*, pp 1-11 (2004)

MIPL-TN-SCT-002 Sunglint Algorithms, DLR Mission Planing – SCOTA, 14.12.2017

Pope, R.M.; Fry, E.S. "Absorption spectrum (380-700 nm) of pure water. II. Integrating cavity measurements", *Applied Optics*, 36, pp. 8710-8723 (1997)

Rozenberg G.V., ed. "Searchlight beam in the atmosphere"(in Russian), *Ac. Sci. USSR*, Moscow, pp. 146-159 (1962)

Richter, R., and Schläpfer D. "Geo-Atmopsheric Processing of Airborne Imaging Spectrometry Data. Part 2: Atmospheric/Topographic Correction." *International Journal of Remote Sensing*, 23, pp. 2631–2649 (2002)

Richter R., Heege T., Kiselev V. and Schlapfer D. "Correction of ozone influence on TOA radiance", *Int. J. Remote Sensing*, 35, pp. 8044-8056 (2014)

Santer R., Schmechtig C., „Adjacency effects on water surfaces: primary scattering approximation and sensitivity study", *Appl. Opt.*, 39(3), pp. 361-375 (2000)

Segelstein, D. "The Complex Refractive Index of Water", *M.S. Thesis, University of Missouri--Kansas City* (1981)

Siewert C.E. "On the singular component of the solution to the searchlight problem in radiative transfer", *J. Quant. Spectr. Radiat. Transfer*, 33(6), pp. 551-554 (1985)

Sushama, L. (project leader), "Evaluating the representation of wind speed Probability Density Functions (PDFs) and the potential wind energy distribution at the local to regional scale using the Canadian RCM", http://www.mrcc.uqam.ca/MITACS/update_wind.pdf (2007)

Vermote E. F., Tanre D., Deuze J. L., Herman M., and Morcette J.-J. "Second Simulation of the Satellite Signal in the Solar Spectrum, 6S: An Overview." *IEEE Transactions on Geoscience and Remote Sensing* 35, pp. 675–686. (1997)

8. List of On-Going TBC & TBD

TBC To Be Confirmed
TBD To Be Determined

Number	Type	Topic	Status	Section	Due date
1	TBC	Interactive in depth analysis of AC module	Resolved/Confirmed	2.8	1.12.2016
2	TBC	Average scene visibility / aerosol optical thickness	Resolved/Confirmed	2.8	1.12.2016
3	TBC	Percentage of water pixels influenced by sun glitter	Resolved/Confirmed	2.8	1.12.2016
4	TBC	Percentage of haze	Resolved/Confirmed	2.8	1.12.2016
5	TBC	Percentage of cloud	Resolved/Confirmed	2,8	1.12.2016

- END OF DOCUMENT -